

Safe Robot Control using Occupancy Grid Map-based Control Barrier Function (OGM-CBF)

Golnaz Raja, Teemu Mökkönen, Reza Ghabcheloo

Abstract—Safe control in unknown environments is a significant challenge in robotics. While Control Barrier Functions (CBFs) are widely used to guarantee system safety, they often assume known environments with predefined obstacles. The proposed method constructs CBFs directly from perception sensor input and introduces a new first-order barrier function for a 3D kinematic robot motion model. The proposed CBF is constructed by combining Occupancy Grid Mapping (OGM) and Signed Distance Functions (SDF). The OGM framework abstracts sensor inputs, making the solution compatible with any sensor modality capable of generating occupancy maps. Moreover, the OGM enhances situational awareness along the robot’s motion trajectory, by integrating both current and previously mapped data. The SDF encapsulates complex obstacle shapes defined by OGM into real-time computable values, enabling the method to handle obstacles of arbitrary shapes. This enables a single constraint in the CBF-QP optimization for each point on the robot, regardless of the number or shape of obstacles. The effectiveness of the proposed approach is demonstrated through simulations on autonomous driving in the CARLA simulator and real-world experiments with an industrial mobile robot, using a simplified 2D version of the method.

Index Terms—Sensor-based Control, Collision Avoidance, Vision-Based Navigation, Autonomous Vehicle Navigation.

I. INTRODUCTION

APPLICATIONS of mobile robots in domains such as autonomous vehicles, industrial robots, and multi-agent systems are often tasked to respect safety while navigating in complex and unknown environments, which stands as one of the most formidable challenges in the field of robotics [1]. One promising approach to integrate safety into design is via Control Barrier Function (CBF) [2] due to the strong mathematical guarantee of satisfying safety requirements. CBFs have been applied in various fields such as legged robots [3], autonomous vehicles [4], multi-robot systems [5], and drones [6]. In recent years, CBF has been combined with Control Lyapunov Functions (CLF) in Quadratic Programs (QP) to ensure both safety and stability in safety-critical systems [7]. Additionally, CBF can act as a QP-based safety filter, modifying unsafe control commands minimally to prevent safety violations [2].

In designing CBF, it is generally assumed that unsafe sets are already known (usually as circular shapes), which is not

applicable to unsafe sets with arbitrary shapes in uncharted environments. Practical implementation of CBF in unknown environments relies on a sufficient awareness of the environment, unsafe regions, and their changes to reach a quick, yet smooth generation of a safety certificate as a response. This requires online estimation of unsafe sets using onboard sensory data and their integration into the CBF formulation as well as advanced frameworks for tuning CBF parameters. For example, in [8], the authors design a neural network, called BarrierNet, to optimize parameters of CBF constructed from sensory data with respect to the user-defined safe sets. Constructing CBF from onboard sensors has been addressed in the literature in through multiple approaches.

One common approach involves detecting the state of obstacles using onboard measurements and then fitting classical circular shapes to the obstacles. This defines the CBF based on the robot’s state, the obstacle’s state, and an approximated radius using traditional methods. In [8], a neural network model was trained to extract the state of obstacles and the robot from front-view images and construct high order CBFs, while tuning their parameters through BarrierNet. The constructed CBFs in this method are dependent on position of obstacles, while simplifying the shape of obstacles via disk fitting. Consequently, using this circular formulation for CBFs, each obstacle requires a separate BarrierNet neuron and constraint, with the number of obstacles needing to be known in advance. In [9], CBF was designed using elliptical outer approximation on occupancy grid maps. The approximation of obstacles with minimum bounding circles in these methods can be overly conservative, and, similarly, this approach requires a separate constraint for each obstacle.

Another approach involves using sensor measurements, such as LiDAR, to approximate signed distance functions (SDFs) and construct CBFs based on the approximated SDF. SDFs provide a smooth, continuous representation of the closest distance to a set’s surface, offering essential information for online obstacle avoidance and motion planning [10]. In [11], safe and unsafe sets are classified using a support vector machine on LiDAR measurements, and the CBF is constructed as the signed distance function of the recovered unsafe set. In this method, the CBF is expressed as a single constraint in the QP optimization, capturing the entire unsafe set. However, the online construction of the unsafe set while accounting for previously observed obstacles requires an exhaustive data collection process, which can become computationally expensive. To address this issue, [12] approximated SDF from

This work was jointly supported by Academy of Finland (SA) 345517, under SA-NSF joint call on artificial intelligence and wireless communication, and Together for RISC-V Technology and Applications (TRISTAN) under Grant 101095947. (Corresponding author: Golnaz Raja.)

All authors are with the Faculty of Engineering and Natural Sciences, Tampere University, 33720 Tampere, Finland. (e-mail: (golnaz.raja@tuni.fi; teemu.mokkonen@tuni.fi; reza.ghabcheloo@tuni.fi).

LiDAR measurements using an incremental training approach with replay memory. In this approach, the online training set includes the latest observations and a randomly sampled subset of previous observations. However, SDF is approximated separately for each obstacle, and consequently, one CBF constraint is needed per obstacle. It is important to note that both of these methods rely on a single sensor modality, LiDAR sensors.

CBF synthesis can also be achieved by classifying safe and unsafe sets in the observation space and defining CBFs directly within that space. In V-CBF [13], semantic segmentation in the image frame is used to capture the shape of obstacles using RGB-D cameras, and a domain translation is applied using cGAN networks to transform the segmented unsafe set into a smooth domain where the CBF is defined. Although this framework successfully enables safe navigation and obstacle avoidance of unknown shapes in uncharted environments, it relies solely on instantaneous sensor inputs from RGB-D cameras and lacks memory of previously encountered obstacles.

In this paper, we introduce a novel method called OGM-CBF, which defines CBF using OGM and SDF. Our contributions are as follows:

- A novel method to construct CBF from perception sensors using Occupancy Grid Mapping (OGM) and Signed Distance Functions (SDF) for robot 3D kinematic motion, and the corresponding novel barrier function leading to first order CBF.
- The OGM component abstracts the sensor input, enabling our method to work with any sensor modality that can generate OGM, a map that safe and unsafe cells are classified.
- The OGM component adds memory enabling our method to integrate sensor data along the motion trajectory increasing situational awareness compared to instantaneous sensor input. Naturally, previously mapped information can also be used.
- In our formulation, SDF encapsulates complex unsafe sets defined by OGM to few numbers that can be computed in real-time, enabling our method to work with obstacles of arbitrary shapes. Robot shape is resolved by calculating SDF at number of representative points on the robot or inflating OGM, and one constraint per point in a QP problem.
- We evaluated the efficacy of the proposed method on safe control of an autonomous driving car in the CARLA simulator as well as an industrial mobile robot in real-world experiments, using a simplified 2D version of our method.

The outline of this paper is as follows: Section II reviews the principles of Control Barrier Function, Occupancy Grid Map, and Signed Distance Function. Section III describes our designed control methodology. Section IV provides a qualitative comparison. Section V is dedicated to the demonstration of the introduced control strategy in the CARLA simulator and on a real robot. Finally, in section VI, the conclusions and future work are provided.

II. PRELIMINARIES AND BACKGROUND

Consider a non-linear control-affine system:

$$\begin{aligned}\dot{\mathbf{x}} &= f(\mathbf{x}) + g(\mathbf{x})\mathbf{u} \\ z &= O_1(\mathbf{x}, \mathbf{q}) \\ (\mathbf{p}, \hat{\mathbf{x}}) &= O_2(\mathbf{x})\end{aligned}\quad (1)$$

where $\mathbf{x} \in \mathbb{X} \subseteq \mathbb{R}^n$ is the state of the system, $\mathbf{u} = [\mathbf{v}, \boldsymbol{\omega}]^T \in \mathbb{U} \subseteq \mathbb{R}^m$ is the control input as linear and angular velocities in body frame, and $f : \mathbb{R}^n \rightarrow \mathbb{R}^n$ and $g : \mathbb{R}^n \rightarrow \mathbb{R}^n$ are locally Lipschitz continuous functions. We assume our robot is equipped with two observation systems O_1 and O_2 . Observation $O_1 : \mathbb{R}^n \times \mathbb{R}^q \rightarrow \mathbb{R}^k$ is a perception sensor capable of generating occupancy grid maps, such as camera, LiDAR, or radar. O_1 is a function of the state and the environment variables $\mathbf{q} \in \mathbb{R}^q$, providing the observation vector $z \in \mathbb{R}^k$. The function $O_2 : \mathbb{R}^n \rightarrow \mathbb{R}^i \times \mathbb{R}^i$ is a function of states and provides position $\mathbf{p} \in \mathbb{R}^i$ and the robot heading unit vector $\hat{\mathbf{x}} \in \mathbb{R}^i$.

Definition 1 (Local Lipschitz continuity): Function $f : D \subseteq \mathbb{R}^n \rightarrow \mathbb{R}^m$ is locally Lipschitz continuous at a point $x \in D$, if there exist constants $M > 0$ and $\delta > 0$ such that for all $x' \in D$ with $\|x - x'\| \leq \delta$, the inequality $\|f(x) - f(x')\| \leq M\|x - x'\|$ is satisfied, with $\|\cdot\|$ denoting the L2 norm.

A. Control Barrier Function

In this paper, we define the safe system as follows:

Definition 2 (Safe system): The system (1) is categorized as safe if $\mathbf{x}(t) \in \mathbb{X}_s \subseteq \mathbb{X}$, $\mathbf{u}(t) \in \mathbb{U}_s \subseteq \mathbb{U}$, $\forall t \geq 0$. Where \mathbb{X}_s is the set of safe states, and \mathbb{U}_s is the set of admissible control inputs.

Consider $S \subseteq \mathbb{X}_s$ to be zero-superlevel set of a continuously differentiable function $h(\mathbf{x}) : \mathbb{X} \rightarrow \mathbb{R}$, yielding:

$$S = \{\mathbf{x} \in \mathbb{X} \mid h(\mathbf{x}) \geq 0\}.\quad (2)$$

To study the safety of system (1), we will use the concept of forward invariant set defined next.

Definition 3 (Forward invariant set): A set S is forward invariant set for the control system (1) if state trajectories starting in S will remain in S for the future time. That is, if $\mathbf{x}(0) \in S$, there exists $\mathbf{u}(t) \in \mathbb{U}_s \subseteq \mathbb{U}$, such that $\mathbf{x}(t) \in S$, $\forall t \geq 0$ [14].

As defined in [2], given the dynamic system (1), the function $h(\mathbf{x})$ is a control barrier function if there exists an extended class κ function $\alpha(\cdot)$ such that for all $\mathbf{x} \in \mathbb{X}$:

$$\sup_{\mathbf{u} \in \mathbb{U}_s} \left[\frac{\partial h(\mathbf{x})}{\partial \mathbf{x}} (f(\mathbf{x}) + g(\mathbf{x})\mathbf{u}) \right] \geq -\alpha(h(\mathbf{x})).\quad (3)$$

We will later use $\dot{h}(\mathbf{x}, \mathbf{u}) = \frac{\partial h(\mathbf{x})}{\partial \mathbf{x}} (f(\mathbf{x}) + g(\mathbf{x})\mathbf{u})$ notation for brevity.

Definition 4 (Extended class κ function): An extended class κ function is a function $\alpha : \mathbb{R} \rightarrow \mathbb{R}$ that is strictly increasing and $\alpha(0) = 0$.

B. Occupancy Grid Map

Occupancy grid maps (OGMs) are fundamental tools in mobile robotics for mapping and navigation. They represent the environment as a tessellated, multi-dimensional grid, with each cell quantifying whether a part of the environment is occupied or not [15]. OGMs are updated and refined over time to improve environmental representation, often using a probabilistic approach to account for uncertainties in sensor measurements [16]. Moreover, OGM is a sensor-agnostic representation which can be updated using measurements from various sensor modalities such as LiDAR, RGB camera [17], stereo camera [18], and radar [19]. Robot pose trajectory is then used to integrate observations over time, succinctly described as follows.

$$m' = M(\mathbf{p}, \hat{\mathbf{x}}, z, m), \quad (4)$$

where \mathbf{p} represents the robot's position, $\hat{\mathbf{x}}$ is the robot's heading, z denotes the sensor measurements from onboard perception sensors, and m is the current belief about the map. The function $M : \mathbb{R}^i \times \mathbb{R}^i \times \mathbb{R}^k \times \mathbb{R}^p \rightarrow \mathbb{R}^p$ updates the map belief m to m' , by integrating new sensor data at the latest pose of the robot into the map. Notice that we need the robot pose (position and heading) to add sensor observations z to current map m to get m' and after generation of the map, map is independent of robots pose and sensor measurement. Sensor extrinsic calibration values (sensor pose in body frame) are used to transform the sensor data into body frame.

To define the safe set, we convert the occupancy grid map m into a binary representation. Equation (5) explains the process of binarizing the occupancy grid map, where μ is defined as the minimum probability (or confidence level) above which a grid cell is considered to be occupied by an obstacle thus unsafe. In other words, μ is the value that determines the acceptance of risk in classifying a grid cell as an obstacle.

$$M_b(m(\mathbf{p})) = \begin{cases} 0 & \text{if } m(\mathbf{p}) < \mu \\ 1 & \text{if } m(\mathbf{p}) \geq \mu \end{cases} \quad (5a)$$

$$(5b)$$

Notice that with slight abuse of notation, we use \mathbf{p} to indicate a cell in the grid map. We can now define the unsafe set \mathbb{X}_u as the union of all states corresponding to the occupied cells of the map, formally,

$$\mathbb{X}_u = \{\mathbf{x} \in \mathbb{X} \mid M_b(m(O_2(\mathbf{x}))) = 1\}. \quad (6)$$

Consequently, the safe set \mathbb{X}_s is given by $\mathbb{X} \setminus \mathbb{X}_u$, which includes all the positions in non-occupied cells of the map.

C. Signed Distance Function

A signed distance function (SDF) is a function that, for a given point \mathbf{p} , outputs the signed distance from \mathbf{p} to the closest point of a set Ω in a metric space. The sign of the distance indicates whether \mathbf{p} is inside or outside Ω [20]. If Ω is a subset of a metric space with metric d , the signed distance function is defined as follows:

$$\phi(\mathbf{p}, \Omega) = \begin{cases} d(\mathbf{p}, \partial\Omega) & \text{if } \mathbf{p} \in \Omega \\ -d(\mathbf{p}, \partial\Omega) & \text{if } \mathbf{p} \notin \Omega \end{cases} \quad (7a)$$

$$(7b)$$

where $\partial\Omega$ denotes the boundary of the set Ω and $d(\mathbf{p}, \partial\Omega)$ represents the minimum distance from \mathbf{p} to points on the boundary. Additionally, $d(\cdot, \partial\Omega)$ is the desired distance metric to the set $\partial\Omega$.

In the case where Ω is a subset of Euclidean space \mathbb{R}^n with a piecewise smooth boundary, and $d(\cdot, \partial\Omega)$ is the Euclidean distance metric, the signed distance function is differentiable almost everywhere. Moreover, the gradient of the function satisfies the eikonal equation $|\nabla\phi| = 1$ at every point where it is differentiable. Interested readers are invited to see more details in [21], [22].

III. CONTROL METHODOLOGY

In this section, we introduce our novel method. Typically, CBF is added as a safety filter to a performance/stabilizing controller. Performance controllers that can be formulated as QP constraints, such as, Control Lyapunov Functions (CLF), can be combined in a QP optimization together with CBF constraints [2]. Formulation of safety controllers and CBF as a QP optimization was an important achievement introduced in [2], paving the way to many proceeding work in safe control, including ours. For our experimental evaluations, we have chosen the CBF-CLF QP formulation. Essential details of this formulation are succinctly provided in this section.

A. Occupancy Grid Map-based Control Barrier Function (OGM-CBF)

Assuming the online occupancy grid map m updating as defined in (4), we will show that the safety is achieved using a control barrier function defined as follows:

$$h(\mathbf{x}) = \Phi_s(\mathbf{p}; \mathbb{X}_s) + l_s + l_a \hat{\mathbf{x}} \cdot \nabla_{\mathbf{p}} \Phi_s(\mathbf{p}; \mathbb{X}_s) \quad (8)$$

where:

- $\Phi_s(\mathbf{p}; \mathbb{X}_s) = T(\phi(\mathbf{p}, \mathbb{X}_s))$, and $T : \mathbb{R}^j \rightarrow \mathbb{R}$ is a odd function for shaping and smoothing, where j is the number of points from the OGM used for interpolation. In other words, Φ_s is a smoothed signed distance function of the set \mathbb{X}_s , evaluated at the robot's body frame position \mathbf{p} .
- $\hat{\mathbf{x}} \cdot \nabla_{\mathbf{p}} \Phi_s(\mathbf{p}; \mathbb{X}_s)$ is the dot product of $\hat{\mathbf{x}}$, and $\nabla_{\mathbf{p}} \Phi_s(\mathbf{p}; \mathbb{X}_s)$, where $\hat{\mathbf{x}}$ is the robot's heading unit vector, $\nabla_{\mathbf{p}} \Phi_s(\mathbf{p}; \mathbb{X}_s)$ is gradient of $\Phi_s(\mathbf{p}; \mathbb{X}_s)$.
- l_s , and l_a are scalar values such that $0 < l_a \leq -l_s$.
- Smoothing/Shaping function T is defined such that $\|\nabla_{\mathbf{p}} \Phi_s(\mathbf{p}; \mathbb{X}_s)\| \leq 1$. This ensures that $\forall \mathbf{x} \in X, l_s + l_a \hat{\mathbf{x}} \cdot \nabla_{\mathbf{p}} \Phi_s(\mathbf{p}; \mathbb{X}_s) \leq 0$,

Note that in above equations, all the quantities such as \mathbf{p} , $\hat{\mathbf{x}}$, and accordingly Φ_s are defined in the same coordinate frame, for instance, the world frame, and \mathbf{p} , $\hat{\mathbf{x}}$ are derived from state of the system as described in (1).

Next, we provide some intuition of the proposed CBF in (8). The proposed CBF function comprises two main components:

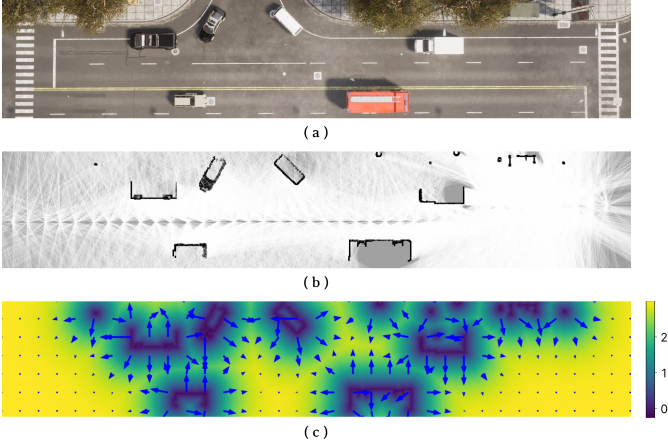


Fig. 1. The process of Φ_s construction. a) Top-view snapshot of the environment in CARLA b) the constructed occupancy grid map c) Φ_s and its gradient field in the map frame

i) The first component captures the effect of the robot's distance to obstacles, and ii) the remaining captures the alignment of the robot's heading vector and the gradient of $\Phi_s(\mathbf{p}; \mathbb{X}_s)$. The larger the components, the safer the robot.

Note that the occupancy grid map m is calculated in discrete positions (centers of the cells). Consequently, due to computational reason and grid representation of m , $\phi(\cdot, \mathbb{X}_s)$ is initially calculated in discrete grid points of the map, and then smoothly interpolated to approximate the SDF at robot position \mathbf{p} (space of real numbers). Function T represents this interpolation (smoothing) and a non-linearity to shape the SDF function. Recall that $|\nabla\phi| = 1$, thus applying T allows adjusting the gradient and scaling of $\phi(\mathbf{p}, \mathbb{X}_s)$ to a desired form. This non-linearity can be applied via functions such as \tanh . Since the norm of the gradient of \tanh is less than 1, all required conditions are satisfied. Moreover, applying the smooth interpolation operator as described ensures the differentiability of $h(\mathbf{x})$. Fig. 1 illustrates the steps involved in constructing Φ_s . In subfigure (a), the CARLA environment is shown in a top-view, which is mapped using a binary OGM in subfigure (b). Finally, Φ_s is constructed as $T(\phi(\cdot, \mathbb{X}_s))$, as visualized in subfigure (c).

The second component, $l_s + l_a \hat{\mathbf{x}} \cdot \nabla_p \Phi_s(\mathbf{p}; \mathbb{X}_s)$, involves calculating the cosine similarity between two vectors: $\hat{\mathbf{x}}$, representing the robot heading, and $\nabla_p \Phi_s(\mathbf{p}; \mathbb{X}_s)$. Notice that $\nabla_p \Phi_s$ is the direction that Φ_s increases the most, thus moving in that direction will move the robot further away from obstacles. The gradient field depicted in Fig. 1 (c) visualizes $\nabla_p \Phi_s(\mathbf{p}; \mathbb{X}_s)$ within the map frame. Notice that l_s is a negative number and the value $-l_s - l_a \geq 0$ is the safety margin, a design choice. The roles of these coefficients become more clear in the proof of Theorem 1. Moreover, notice that without the second component, derivative of $h(\mathbf{x})$ will be only a function of linear velocity, that is, to maintain the safety, the system can only stop. To enable steering, the solution is to

use a higher order CBF [23] thus additional complexity. By adding the second term, the angular velocity appears in the first derivative of $h(\mathbf{x})$, and allows also steering around obstacles. A similar idea was used in [24].

Now, we can establish how the constructed function has the necessary properties to be a control barrier function.

Theorem 1: Set $S = \{\mathbf{x} \in \mathbb{X} \mid h(\mathbf{x}) \geq 0\}$ with $h(\mathbf{x})$ defined in (8) is a forward-invariant set and $h(\mathbf{x})$ is a control barrier function for system (1), with $\mathbf{u} = [\mathbf{v}, \boldsymbol{\omega}]^T$ as the control input.

Proof: We will first show that $S \subseteq \mathbb{X}_s$. The condition on T and $0 < l_a \leq -l_s$ ensure that $\forall \mathbf{x}$ we have $c \equiv l_s + l_a \hat{\mathbf{x}} \cdot \nabla_p \Phi_s(\mathbf{p}; \mathbb{X}_s) \leq 0$. For any $\mathbf{x} \in S = \{\mathbf{x} : h(\mathbf{x}) \geq 0\}$, we have $h(\mathbf{x}) \geq 0$, therefore $\Phi_s(\mathbf{p}; \mathbb{X}_s) = h(\mathbf{x}) - c \geq 0$, and consequently $\phi(\mathbf{p}, \mathbb{X}_s) \geq 0$, since $T(\cdot)$ is an odd function. Thus $\mathbf{x} \in \mathbb{X}_s = \{\mathbf{x} : \phi(\mathbf{p}, \mathbb{X}_s) \geq 0\}$, proving the first part.

We will now show that there are control signals \mathbf{u} such that (3) is satisfied. We will first derive $\dot{h}(\mathbf{x}, \mathbf{u})$. Time derivative of h is

$$\dot{h} = \frac{d}{dt} \Phi_s(\mathbf{p}; \mathbb{X}_s) + \frac{d}{dt} (l_a \hat{\mathbf{x}} \cdot \nabla_p \Phi_s(\mathbf{p}; \mathbb{X}_s)), \quad (9)$$

and assuming the environment is stationary (\mathbb{X}_s is not changing), we have

$$\dot{h} = \nabla_p \Phi_s \cdot \dot{\mathbf{p}} + l_a \frac{d\hat{\mathbf{x}}}{dt} \cdot \nabla_p \Phi_s + l_a \hat{\mathbf{x}} \cdot \frac{d}{dt} \nabla_p \Phi_s. \quad (10)$$

Note that $\hat{\mathbf{x}} = R\hat{\mathbf{e}}$, where R is the rotation matrix expressing the body in the world frame, and $\hat{\mathbf{e}} = [1, 0, 0]$ the x-axis of the world frame. Given that $\dot{\mathbf{p}} = R\mathbf{v}$ and $\frac{d\hat{\mathbf{x}}}{dt} = R[\boldsymbol{\omega}]\hat{\mathbf{e}}$, the equation (10) can be written as $\dot{h} = a(\mathbf{x})\mathbf{v} + b(\mathbf{x})\boldsymbol{\omega}$. Since, $(\mathbf{v}, \boldsymbol{\omega})$ can be made zero, condition (3) can be satisfied and thus $h(\mathbf{x})$ is a control barrier function for (1), and S is an invariant set. ■

Considering the control system in (1), with control inputs $\mathbf{u} = [\mathbf{v}, \boldsymbol{\omega}]^T$, the control policy outlined in (11) ensures safety across all trajectories originating within S .

$$\pi_{ogm-cbf} = \{(\mathbf{v}, \boldsymbol{\omega}) \in \mathbb{U}_s \mid a(\mathbf{x})\mathbf{v} + b(\mathbf{x})\boldsymbol{\omega} \geq -\alpha(h(\mathbf{x}))\} \quad (11)$$

It is important to recognize that the efficacy of the safety controller is influenced by the design of the function $T(\cdot)$, $\alpha(\cdot)$, and the values of l_s , and l_a , which can be adjusted according to the model of the system, the dimensions of the map, and the environment.

B. Control Lyapunov Function (CLF)

In addition to ensuring safety, it is imperative to establish a control objective. Consider a candidate Control Lyapunov Function (CLF) for this purpose, denoted as $V : \mathbb{X} \rightarrow \mathbb{R}$, characterized by continuous differentiability and positive definiteness.

Definition 5: Consider a function $V : \mathbb{X} \rightarrow \mathbb{R}$ to be positive-definite over the domain \mathbb{X} provided that: (i) $V(0) = 0$, and (ii) for any $\mathbf{x} \in \mathbb{X}$ with $\mathbf{x} \neq 0$, it holds that

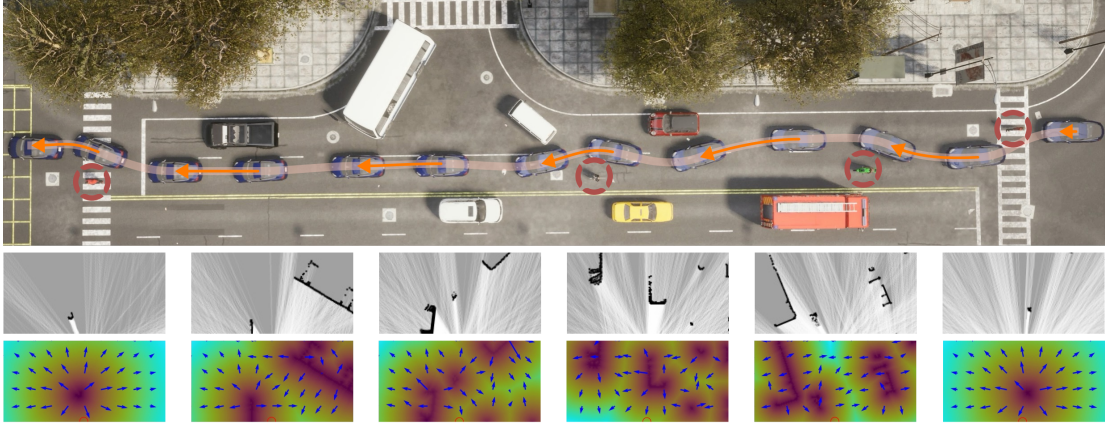


Fig. 2. Top-view snapshot of the simulation in the CARLA environment. The black car is a self-driving vehicle using OGM-CBF to navigate safely. The orange dashed line represents the path of the autonomous car. The second row shows the upper half of the egocentric local occupancy grid map denoted as m , and the last line illustrates Φ_s and its gradient field in the map frame during the experiment.

$V(\mathbf{x}) > 0$.

As mentioned in [2], the stability of (1) in equilibrium point can be achieved with a necessary and sufficient condition as follows:

$$\inf_{\mathbf{u} \in \mathbb{U}} [\dot{V}(\mathbf{x}, \mathbf{u}) = \frac{\partial V}{\partial \mathbf{x}}(f(\mathbf{x}) + g(\mathbf{x})\mathbf{u})] \leq -\gamma(V(\mathbf{x})) \quad (12)$$

where $\gamma(\cdot)$ is defined as an extended class κ function. Consequently, the subsequent control strategy will ensure the stability requirements:

$$\pi_{clf} = \{\mathbf{u} \in \mathbb{U}_s \mid \dot{V}(\mathbf{x}, \mathbf{u}) \leq -\gamma(V(\mathbf{x}))\} \quad (13)$$

C. Integrating CLF and OGM-CBF

To ensure both safety and stability, the proposed control policy is defined as the intersection $\pi^* = \pi_{ogm-cbf} \cap \pi_{clf}$. If the intersection is empty, safety is prioritized. This leads to the following constrained optimization problem, balancing safety and stability as hard and soft constraints, respectively.

$$\mathbf{u}^* = \underset{\mathbf{u}}{\operatorname{argmin}} J(\mathbf{u}, \mathbf{x}, \delta) \quad (14a)$$

$$\text{s.t. : } \dot{V}(\mathbf{x}, \mathbf{u}) \leq \gamma(V(\mathbf{x})) + \delta \quad (14b)$$

$$\dot{h}(\mathbf{x}, \mathbf{u}) \geq -\alpha(h(\mathbf{x})) \quad (14c)$$

$$\mathbf{u}_{lb} \leq \mathbf{u} \leq \mathbf{u}_{ub}, \quad (14d)$$

where J represents the cost function, while \mathbf{u}_{lb} and \mathbf{u}_{ub} are the lower and upper bounds of the control input, respectively. Additionally, δ is introduced as the relaxation parameter, activated when constraints conflict, resulting in an empty intersection between $\pi_{ogm-cbf}$ and π_{clf} . Under such circumstances, the hard constraint (related to safety) is maintained, whereas the soft constraint (related to stability) is moderated.

Since system (1) is affine in u , both \dot{V} and \dot{h} will become control-affine, more specifically

$$\dot{V}(\mathbf{x}, \mathbf{u}) = a_1(\mathbf{x}) + b_1(\mathbf{x})\mathbf{u} \quad (15a)$$

$$\dot{h}(\mathbf{x}, \mathbf{u}) = a_2(\mathbf{x}) + b_2(\mathbf{x})\mathbf{u} \quad (15b)$$

for some $a_i(\mathbf{x}), b_i(\mathbf{x}), i = 1, 2$. A quadratic cost function J used in our experiments is

$$J = (\mathbf{u} - \mathbf{u}_{ref}(\mathbf{x}))^T (\mathbf{u} - \mathbf{u}_{ref}(\mathbf{x})) + \delta^2 \quad (16a)$$

Since J is quadratic and constraints are linear in (\mathbf{u}, δ) , the optimization (14) is a Quadratic Programs (QP). Algorithm (1) details the steps of deployment of the proposed OGM-CBF. In the algorithm, we assume that, given the observations, we can calculate state-dependent variables $\mathbf{u}_{ref}(\mathbf{x}), V(\mathbf{x}), h(\mathbf{x}), a_i(\mathbf{x}), b_i(\mathbf{x}),$ for $i = 1, 2$.

Algorithm 1: Map-based Safety Control Algorithm

Input: observations z, \mathbf{p} , and $\hat{\mathbf{x}}$

Output: Control Input: \mathbf{u}

1 **while** Robot is running **do**

2 receive observations z, \mathbf{p} , and $\hat{\mathbf{x}}$

3 update occupancy grid map m and safe set \mathbb{X}_s

4 calculate $\Phi_s(\mathbf{p}; \mathbb{X}_s)$ and its gradient

5 calculate $\mathbf{u}_{ref}(\mathbf{x}), V(\mathbf{x}), h(\mathbf{x}),$

$a_i(\mathbf{x}), b_i(\mathbf{x}), i = 1, 2$

6 run optimization (14) to obtain control inputs: \mathbf{u}^*

IV. QUALITATIVE COMPARISON

In this section, we clarify some of our contributions, compared to prior art.

Sensor Agnostic: OGM-CBF uses OGM to generate safe and unsafe sets. OGM can be constructed with sensors like LiDAR, radar, and cameras, making it adaptable to various sensors and environmental features. In contrast, [11]–[13] rely

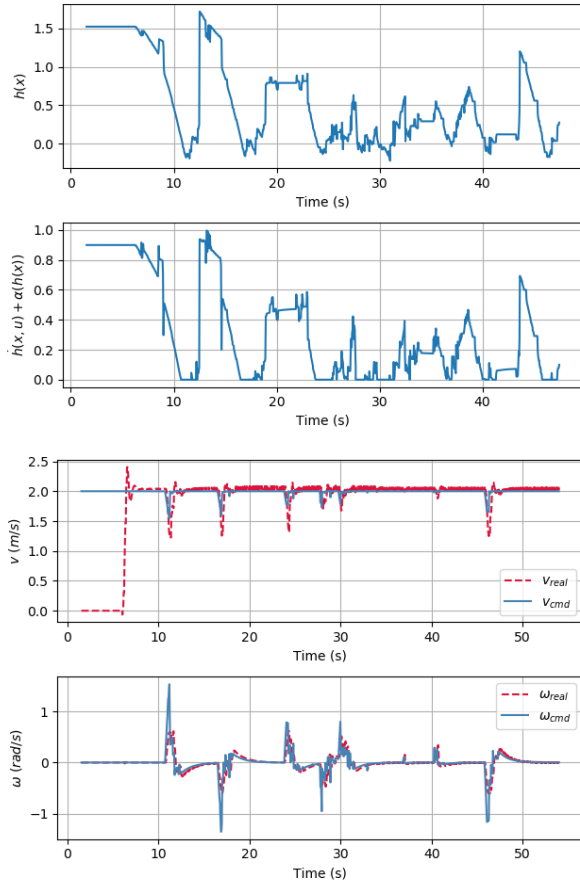


Fig. 3. $h(\mathbf{x})$ (first), $\hat{h}(\mathbf{x}, \mathbf{u}) + \alpha(h(\mathbf{x}))$ (second), Linear (third) and angular velocity (forth) of the autonomous vehicle vs. time in the CARLA simulator. The devised commands by the controller are visualized with a solid line, while real measurements are shown using a dashed line.

solely on one sensor modality, limiting their effectiveness in challenging conditions, such as poor lighting or reflective surfaces for RGB-D sensors and adverse weather conditions for LiDARs, where they are prone to extreme noise.

Spatial Awareness: OGM accumulates sensor data over time, providing a comprehensive and continuously updated environmental map for OGM-CBF, unlike V-CBF [13], which relies on instantaneous measurements. In [13], CBF’s awareness of the obstacles only relies on the current coverage of sensors (RGB-D cameras). In [11], previously constructed unsafe set is considered in CBF, while storing all the previous sensor measurements for online training of unsafe set detection, which is computationally expensive. To address this challenge, [12] leverages incremental online training with replay memory in SDF approximation.

Robustness: There are two sources of uncertainties: (i) perception sensors, and (ii) the robot pose/state estimation. OGM takes into account both uncertainties during the creation of the map. Moreover, when the localization is too uncertain, even if the map is created a priori with more accurate systems, to retain robust safety OGM-CBF provides the designer with

possibility to tune l_a and l_s for an extra safety margin. Therefore, our method is robust in that sense, compared to [13] [12], which has no mechanism to handle sensor uncertainties. In [11] a robustness to sensor noise is provided in the SVM formulation.

Efficacy: In [13], [12], [25], [9], one constraint is needed per obstacle. In contrast, in OGM-CBF and similarly in [11], with the effective use of SDFs, a single constraint can account for all detected obstacles, making it more efficient for real-time deployment.

V. EXPERIMENTAL EVALUATION

In this section, we will demonstrate the effectiveness of the introduced control strategy on a self-driving car in the CARLA autonomous driving simulator [26] and on an industrial mobile robot.

A. CARLA

The experiment aims to validate the safe navigation of an autonomous car using OGM-CBF in a scenario including diverse obstacles. In this case, the state of the system is $\mathbf{x} = [x, y, \psi]^T$ (the coordinates of the vehicle’s center in the 2D plane, and the heading of the vehicle), and the workspace of the system is two dimensional, with $\mathbf{u} = [v, \omega]^T$ (linear and angular speeds) as the control inputs. Steering and throttle commands are calculated using the standard kinematic bicycle model in a 2D workspace [27]. A LiDAR sensor is mounted on the ego vehicle to generate the occupancy grid map m online, where each grid cell represents a 0.1 by 0.1 meter area of the environment. The LiDAR sensor’s range is 70 meters, with 760000 points per scan and 35 degrees field of view, and the map binarization threshold $\mu = 0.5$. The simulation involves navigating through an unknown environment cluttered with various stationary obstacles, such as cars and pedestrians.

Our control objective is to maintain the vehicle heading and avoid obstacles. Safe navigation is deployed by a controller based on Algorithm (1) and the optimization framework (14). The performance controller is defined by an output tracking error as a Lyapunov function $V(\mathbf{x}) = \frac{1}{2}(\psi - \psi_{ref})^2$, where ψ is the robot heading (angle of \hat{x}), while the optimization’s cost function is $J(\mathbf{u}, \mathbf{x}, \delta) = \frac{1}{2}(v - v_{ref})^2 + \frac{1}{2}(\omega - \omega_{ref})^2 + \delta^2$, where reference velocities are $v_{ref} = 2m/s$, $\omega_{ref} = -k(\psi - \psi_{ref})$. The controller’s effectiveness can be inspected from Fig. 2. In this Figure, in the first row, the orange line shows the path of the ego vehicle. In addition to cars, smaller obstacles such as pedestrians, bicyclists, and motorcyclists are spawned in the environment (marked with red circles). During the experiment, OGM-CBF utilizes an upper half of the ego-centric local occupancy grid map as m , shown in the second row. And the last row displays Φ_s and the gradient field of it in the map frame.

Additionally, as the robot has a positive lower bound velocity, $T(\phi(\mathbf{p}, \mathbb{X}_s))$ is only constructed for the upper half of the ego-centric map as the function $c(a \tanh(b\phi(\mathbf{p}, \mathbb{X}_s)))$, where $a = 3$ and $b = 0.01$ are tuned based on the desired behaviour, and $c(\cdot)$ is a polynomial interpolation function

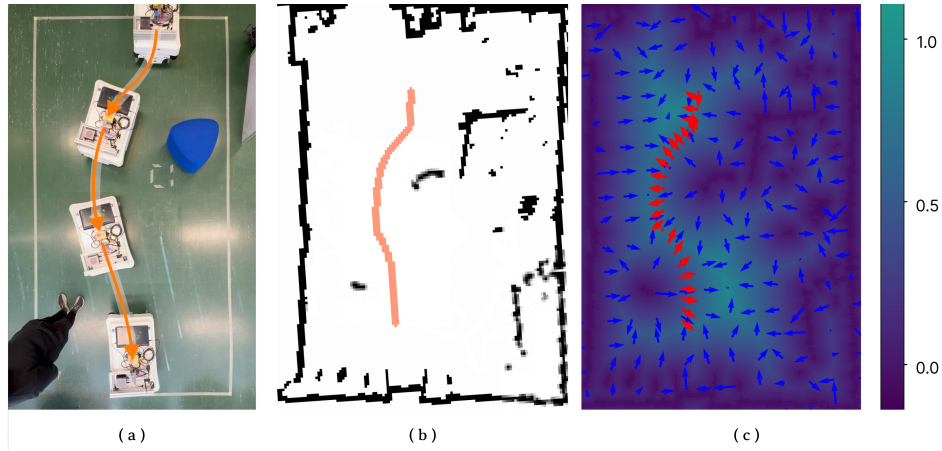


Fig. 4. Safe navigation of MiR100 using OGM-CBF. a) 2D snapshot of the robot during the experiment, b) the constructed occupancy grid map using onboard sensors, c) Φ_s and its gradient field in the map frame. The orange line shows the path of the robot and the red gradients represent the gradient values used by the algorithm during the experiment.

as described in section III-A. Moreover, $l_s = -0.5$ and $l_a = 0.5$. Fig. 3 quantitatively illustrates that the designed controller in fact navigates safely during the experiment. The first row displays the value of $h(\mathbf{x})$, and the second row shows $\dot{h}(\mathbf{x}, \mathbf{u}) + \alpha(h(\mathbf{x}))$, which remains non-negative, indicating constant satisfaction of the safety constraint. The third and fourth rows depict the control inputs $\mathbf{u} = [v, \omega]^T$ generated by Algorithm (1) (solid lines), alongside the actual linear and angular velocities of the vehicle (dashed lines) with respect to time. Note the value of $h(\mathbf{x})$ can become negative near obstacles due to the approximation of the system (1) as a kinematic model.

B. Real-world

Besides simulated validation, additional experiments were conducted on an industrial mobile robot (MiR100), which is a differential wheeled robot equipped with an Nvidia Jetson AGX Orin and two onboard compact safety laser scanner SICK S300, with scanning angle of 270 degrees. The system is considered with 2D workspace, same as Section V-A. Mapping and safe control are deployed using the ROS2 framework on this platform, and localization is done internally using onboard sensors.

In this experiment, the robot utilizes a pre-established global map of the environment, which is dynamically updated with an average frequency of 16.372 Hz using real-time sensor measurements collected from laser scanners. Each grid cell in the map covers a 0.05 by 0.05 meter section of the environment with map binarization threshold of $\mu = 0.5$. Safe navigation is managed by a controller based on Algorithm (1) using OGM-CBF and the optimization framework (14), with the same quadratic Lyapunov function and cost function as in Section V-A, which is similarly utilized to maintain the desired heading and $v_{ref} = 0.25$. The employed controller runs on the platform with an average frequency of 12.498 Hz, and the applied function $T(\phi(\mathbf{p}, \mathbb{X}_s))$ is the same as in the

CARLA experiments, with $a = 3$ and $b = 0.01$. Moreover, $l_s = -0.35$ and $l_a = 0.35$.

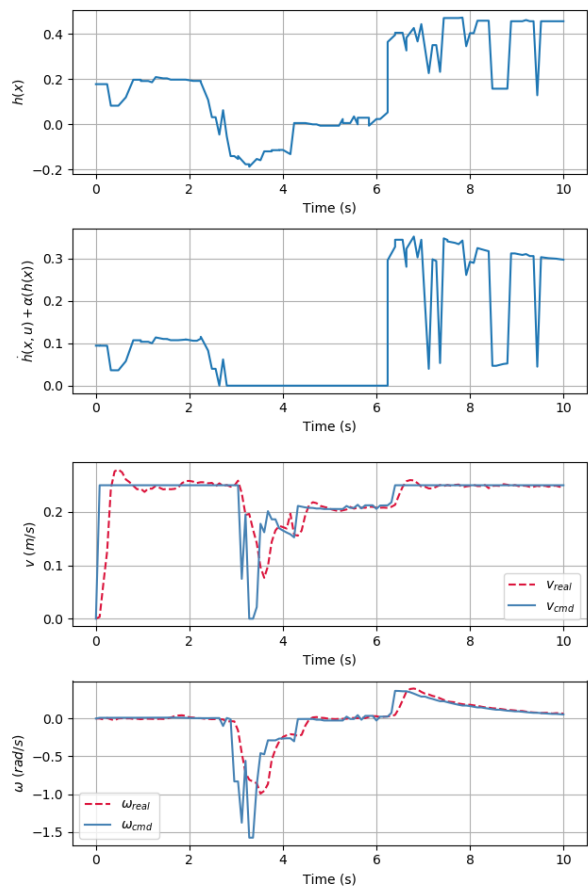


Fig. 5. $h(\mathbf{x})$ (first), $\dot{h}(\mathbf{x}, \mathbf{u}) + \alpha(h(\mathbf{x}))$ (second), Linear (third) and angular velocity (fourth) of the mobile robot vs. time. The controller's commands are displayed using a solid line, whereas the real measurements are indicated with a dashed line.

Fig. 4 shows the robot's path (orange lines) during the experiment. The subfigure (a) demonstrates OGM-CBF's capabilities to avoid obstacles with arbitrary shapes (the black obstacle and a human). (b) shows the global occupancy grid map updated in real-time by laser scanners, and the robot's path in the map frame. (c) presents Φ_s and its gradient field in the map frame (black arrows). Moreover, the gradients of Φ_s along the robot's path are marked by red arrows, indicating the direction of avoidance near obstacles utilized in the controller.

Fig. 5 quantitatively validates the robot's safe navigation using OGM-CBF during the experiment. The first row displays the value of $h(\mathbf{x})$, the second row presents $\dot{h}(\mathbf{x}, \mathbf{u}) + \alpha(h(\mathbf{x}))$, and the final two rows illustrate the commanded (solid black line) and actual (dashed red line) linear and angular velocities of the robot with respect to time.

As values in Fig. 5 illustrate, the robot is able to satisfy the safety constraint of OGM-CBF and navigate safely in the environment. Note that as the system (1) is considered kinematically, $h(\mathbf{x})$ goes to negative values in proximity to obstacles. However, the controller increases the value of $h(\mathbf{x})$ successfully by generating proper control commands.

VI. CONCLUSION

This paper introduces OGM-CBF, a novel method for safe robot navigation in both known and unknown environments. By combining Control Barrier Functions (CBF) with Occupancy Grid Maps (OGM) and Signed Distance Functions (SDF), the method efficiently handles arbitrary obstacle shapes and sensor inputs. OGM-CBF is implemented as a single constraint in a Quadratic Programming (QP) formulation. Validation in the CARLA simulator and on an industrial mobile robot demonstrates reliable autonomous navigation. Future work will focus on considering actuator dynamics in the CBF design, and including a method for parameter tuning given certain desired robot behaviour in the presence of obstacles.

REFERENCES

- [1] G.-Z. Yang, J. Bellingham, P. E. Dupont, P. Fischer, L. Floridi, R. Full, N. Jacobstein, V. Kumar, M. McNutt, R. Merrifield, *et al.*, "The grand challenges of science robotics," *Science robotics*, vol. 3, no. 14, p. eaar7650, 2018.
- [2] A. D. Ames, S. Coogan, M. Egerstedt, G. Notomista, K. Sreenath, and P. Tabuada, "Control barrier functions: Theory and applications," in *2019 18th European control conference (ECC)*, pp. 3420–3431, IEEE, 2019.
- [3] Q. Nguyen, A. Hereid, J. W. Grizzle, A. D. Ames, and K. Sreenath, "3d dynamic walking on stepping stones with control barrier functions," in *2016 IEEE 55th Conference on Decision and Control (CDC)*, pp. 827–834, IEEE, 2016.
- [4] A. D. Ames, J. W. Grizzle, and P. Tabuada, "Control barrier function based quadratic programs with application to adaptive cruise control," in *53rd IEEE Conference on Decision and Control*, pp. 6271–6278, IEEE, 2014.
- [5] L. Wang, A. D. Ames, and M. Egerstedt, "Safety barrier certificates for collisions-free multirobot systems," *IEEE Transactions on Robotics*, vol. 33, no. 3, pp. 661–674, 2017.
- [6] A. Singletary, A. Swann, Y. Chen, and A. D. Ames, "Onboard safety guarantees for racing drones: High-speed geofencing with control barrier functions," *IEEE Robotics and Automation Letters*, vol. 7, no. 2, pp. 2897–2904, 2022.

- [7] A. D. Ames, X. Xu, J. W. Grizzle, and P. Tabuada, "Control barrier function based quadratic programs for safety critical systems," *IEEE Transactions on Automatic Control*, vol. 62, no. 8, pp. 3861–3876, 2016.
- [8] W. Xiao, T.-H. Wang, R. Hasani, M. Chahine, A. Amini, X. Li, and D. Rus, "Barriernet: Differentiable control barrier functions for learning of safe robot control," *IEEE Transactions on Robotics*, 2023.
- [9] J. Liu, M. Li, J. W. Grizzle, and J.-K. Huang, "Clf-cbf constraints for real-time avoidance of multiple obstacles in bipedal locomotion and navigation," in *2023 IEEE/RSJ International Conference on Intelligent Robots and Systems (IROS)*, pp. 10497–10504, IEEE, 2023.
- [10] L. Han, F. Gao, B. Zhou, and S. Shen, "Fiesta: Fast incremental euclidean distance fields for online motion planning of aerial robots," in *2019 IEEE/RSJ International Conference on Intelligent Robots and Systems (IROS)*, pp. 4423–4430, IEEE, 2019.
- [11] M. Srinivasan, A. Dabholkar, S. Coogan, and P. A. Vela, "Synthesis of control barrier functions using a supervised machine learning approach," in *2020 IEEE/RSJ International Conference on Intelligent Robots and Systems (IROS)*, pp. 7139–7145, IEEE, 2020.
- [12] K. Long, C. Qian, J. Cortés, and N. Atanasov, "Learning barrier functions with memory for robust safe navigation," *IEEE Robotics and Automation Letters*, vol. 6, no. 3, pp. 4931–4938, 2021.
- [13] H. Abdi, G. Raja, and R. Ghabcheloo, "Safe control using vision-based control barrier function (v-cbf)," in *2023 IEEE International Conference on Robotics and Automation (ICRA)*, pp. 782–788, IEEE, 2023.
- [14] F. Blanchini, "Set invariance in control," *Automatica*, vol. 35, no. 11, pp. 1747–1767, 1999.
- [15] H. Moravec and A. Elfes, "High resolution maps from wide angle sonar," in *Proceedings. 1985 IEEE international conference on robotics and automation*, vol. 2, pp. 116–121, IEEE, 1985.
- [16] T. Collins and J. Collins, "Occupancy grid mapping: An empirical evaluation," in *2007 mediterranean conference on control & automation*, pp. 1–6, IEEE, 2007.
- [17] Y. Wei, L. Zhao, W. Zheng, Z. Zhu, J. Zhou, and J. Lu, "Surroundoc: Multi-camera 3d occupancy prediction for autonomous driving," in *Proceedings of the IEEE/CVF International Conference on Computer Vision*, pp. 21729–21740, 2023.
- [18] T.-N. Nguyen, B. Michaelis, A. Al-Hamadi, M. Tornow, and M.-M. Meinecke, "Stereo-camera-based urban environment perception using occupancy grid and object tracking," *IEEE Transactions on Intelligent Transportation Systems*, vol. 13, no. 1, pp. 154–165, 2011.
- [19] M. Li, Z. Feng, M. Stolz, M. Kunert, R. Henze, and F. Küçükay, "High resolution radar-based occupancy grid mapping and free space detection," in *VEHITS*, pp. 70–81, 2018.
- [20] T. Chan and W. Zhu, "Level set based shape prior segmentation," in *2005 IEEE Computer Society Conference on Computer Vision and Pattern Recognition (CVPR'05)*, vol. 2, pp. 1164–1170, IEEE, 2005.
- [21] C. Dapogny and P. Frey, "Computation of the signed distance function to a discrete contour on adapted triangulation," *Calcolo*, vol. 49, pp. 193–219, 2012.
- [22] H. Luo, X. Wang, and B. Lukens, "Variational analysis on the signed distance functions," *Journal of Optimization Theory and Applications*, vol. 180, pp. 751–774, 2019.
- [23] W. Xiao and C. Belta, "Control barrier functions for systems with high relative degree," in *2019 IEEE 58th conference on decision and control (CDC)*, pp. 474–479, IEEE, 2019.
- [24] N. E. Toulkani, H. Abdi, O. Koskelainen, and R. Ghabcheloo, "Reactive safe path following for differential drive mobile robots using control barrier functions," in *2022 10th International Conference on Control, Mechatronics and Automation (ICMA)*, pp. 60–65, IEEE, 2022.
- [25] W. Xiao, T.-H. Wang, M. Chahine, A. Amini, R. Hasani, and D. Rus, "Differentiable control barrier functions for vision-based end-to-end autonomous driving," *arXiv preprint arXiv:2203.02401*, 2022.
- [26] A. Dosovitskiy, G. Ros, F. Codevilla, A. Lopez, and V. Koltun, "Carla: An open urban driving simulator," in *Conference on robot learning*, pp. 1–16, PMLR, 2017.
- [27] R. Rajamani, *Vehicle dynamics and control*. Springer Science & Business Media, 2011.